# Electrical properties of stoichiometric $BiFeO_3$ prepared by mechanosynthesis with either conventional or spark plasma sintering

Antonio Perejón[1], Nahum Masó[2], Anthony R. West[2], Pedro E. Sánchez-Jiménez[1], Rosalía Poyato[1], José M. Criado[1] and Luis A. Pérez-Maqueda[1]

[1] Instituto de Ciencia de Materiales de Sevilla (CSIC-US), AmericoVespucio 49, 41092 Sevilla, Spain

[2] Department of Materials Science and Engineering, University of Sheffield, S1 3JD, Sheffield, UK.

## Abstract

Phase-pure powders of stoichiometric $BiFeO_3$ have been prepared by mechanosynthesis. Ceramics sintered by either conventional heating in air or spark plasma sintering (SPS) followed by oxidative anneal in air are highly insulating with conductivity e.g. $\sim 10^{-6}$ $Scm^{-1}$ at 300 °C and activation energy 1.15(2) eV, which are comparable to those of a good-quality $BiFeO_3$ single crystal. By contrast, the as-prepared SPS sample without the post-sinter anneal shows higher conductivity e.g. $\sim 10^{-6}$ $Scm^{-1}$ at 225 °C and lower activation energy 0.67(3) eV, indicating some reduction of the sample by the SPS process. The reason for the high conductivity observed in some ceramic samples reported in the literature appears to be unclear at present.

## Introduction

Bismuth ferrite ($BiFeO_3$) is one of the most studied multiferroic ceramics since multifunctional properties are present at room temperature; it exhibits a G-type antiferromagnetic order up to the Néel temperature at ~360 ºC and ferroelectric order up to the Curie temperature at ~ 830 ºC. [1, 2] However, phase-pure bulk $BiFeO_3$ is notoriously difficult to synthesise and it is very common that small amounts of persistent secondary phases, mostly $Bi_2Fe_4O_9$ and $Bi_{25}FeO_{39}$, are present. Thus, although many methods have been proposed in the literature [3–19] to obtain phase-pure bulk $BiFeO_3$, only few have been successful.

An alternative approach for preparing phase-pure bulk $BiFeO_3$ is by mechanochemical synthesis. Nanoparticles of $BiFeO_3$ are obtained by mechanical alloying stoichiometric amounts of iron and bismuth oxides. [20–22] Recently, some of the present authors have investigated the effect of milling conditions on the composition and microstructure of the resulting materials, and shown that the microstructure of the products could be tailored by selecting the milling conditions. Interestingly, materials prepared by mechanosynthesis have been sintered without the formation of secondary phases. [22]

There is considerable disagreement in the literature concerning the electrical properties of $BiFeO_3$. It is well-established that it is both ferroelectric and antiferromagnetic at room temperature but there is no consistency in reported values of its electrical conductivity; semiconducting ceramics with low electrical resistivity at room temperature are frequently obtained. In order to improve the insulating properties of $BiFeO_3$, small amounts of donor dopants [23, 24] such as $Ti^{4+}$ substituting for $Fe^{3+}$ are usually added to suppress the semiconductivity.

The low electrical resistivity of $BiFeO_3$ has been linked to the presence of impurities [3] which is one of the most important problems for future applications of this material in spintronics or data storage. One objective of this work has been to investigate the electrical properties of stoichiometric pure $BiFeO_3$ prepared by direct mechanochemical synthesis from pristine iron and bismuth oxides. The effect of sintering under both conventional conditions and by spark plasma sintering, as well as the effects of cooling rate and oxygen partial pressure on the resulting electrical properties, was also proposed for study.

**Experimental**

Samples of $BiFeO_3$ prepared by mechanosynthesis were obtained from $Bi_2O_3$ (Sigma-Aldrich 223891-500G, 10 μm, 99.9% pure) and $Fe_2O_3$ (Sigma-Aldrich 310050-500G, <5 μm, ≥99% pure). Stoichiometric amounts of the oxides were mechanically treated in a modified planetary ball mill Fritsch Pulverisette 7 (Idar-Oberstein, Germany) under 7 bars of oxygen pressure. The mill was modified by incorporating a rotary valve that allows connection of the jar (sealed with a Viton o-ring and equipped with a male taper straight adaptor) and the gas cylinder during milling. Thus, the pressure inside the jar could be maintained constant during the entire treatment even if gas was consumed by the reaction. In all experiments, the jars were purged several times with oxygen and the desired pressure selected and maintained during milling. The spinning rates of both the supporting disc and the superimposed rotation in the opposite direction of the jar was set at 700 rpm and the powder-to-ball mass ratio was set at 1:20.

Two methods were used to obtain pellets of the mechanosynthesised samples: conventional sintering and spark plasma sintering (SPS, Model 515S; SPS Dr Sinter Inc., Kanagawa, Japan). Conventional sintering consisted of pressing the milled powders into discs, ~6 mm in diameter and ~2 mm thick by uniaxial pressing at 0.93 GPa and heated at 10 °C $min^{-1}$ to 850 °C in air and then slow-cooled by switching off the furnace. The SPS of the powder was performed in vacuum in a 10 mm diameter cylindrical graphite die/punch setup, under a uniaxial pressure of 75 MPa at 625 ºC for 10 minutes. The heating rate was 250 ºC $min^{-1}$. Temperature was measured using a thermocouple, which was placed in a bore hole in the middle part of the graphite die. The sintered ceramics, ~10 mm in diameter and ~2 mm thick were polished to eliminate carbon from the surface. Density of the ceramics was determined using the Archimedes' method, using water as the immersion liquid. Pellet densities were ~95(3) %, Table I.

For selected experiments, samples were heated: a) at 800 °C for 30 min in air followed by quenching; b) in $O_2$ at ~125 bar for 60 min in a Morris high pressure furnace (HOP) followed by slow cooling at 1 °C$min^{-1}$; c) at 350–600 $^{o}$C in vacuum at 5x$10^{-5}$ mbars.

For comparison purposes, samples of $BiFeO_3$ prepared by conventional solid state reaction used powders, and drying temperatures, of $Bi_2O_3$ (99.99% pure, Acros Chemicals, 180 °C) and $Fe_2O_3$ (99% pure, Sigma-Aldrich, 400 °C). These were mixed in an agate mortar and pestle for ~30 min, with acetone added periodically to form a paste. Pellets were pressed uniaxially and placed on sacrificial powder of the same composition in alumina boats. Initial firing was at 850 °C for 20 min after which the pellets were ground, repressed, fired again at 850 °C for 20 min, ground, repressed isostatically at 200 MPa, given a final firing at 850 °C for 2 h in air and then cooled slowly by switching off the furnace.

The phases present were analyzed by X-Ray Powder Diffraction (XRD) using either a Stoe StadiP Diffractometer (Darmstadt, Germany) or a Panalytical X'Pert Pro diffractometer (Almelo, The Netherlands). Lattice parameters were determined by least-squares refinement for reflections in the range $15 < 2\theta < 80^{o}$, using the software WinXPow version 1.06, and an external Si standard. The sizes of the coherently diffracting domains were calculated from the (024) diffraction peak by the line profile analysis (Panalytical X'Pert Pro software, Almelo, The Netherlands) corrected for instrumental peak broadening determined with a Si standard. Elemental composition of the samples was assayed by X-ray fluorescence analysis using a Panalytical Axios XRF Spectrometer (Almelo, The Netherlands) equipped with a Rh tube.

The microstructure of the powders and the pellets was studied by scanning electron microscopy (SEM). The micrographs were obtained in a Hitachi S-4800 microscope (Tokyo, Japan) equipped with energy dispersive X-ray spectrometer (EDAX) attachment. Differential scanning calorimetry

(DSC) measurements were performed in a Netzsch DSC404C (Selb, Germany) from room temperature to 850 ºC with heating/cooling rates 10 °C $min^{-1}$. In order to study possible variation in oxygen content as a function of heat treatment conditions, thermogravimetry (TG) measurements were carried out in a home-made thermogravimetric instrument [25] from room temperature to either 350–600 $^{o}$C in vacuum ($5x10^{-5}$ mbars) at heating/cooling rates 5 °C $min^{-1}$ or to 600 $^{o}$C in air in a TA instruments Q5000IR (New Castle, DE, USA).

For electrical property measurements, pellets were Au sputter coated using an Emitech K575X Sputter Coater (Kent, UK). Impedance measurements used a combination of Agilent 4294A and E4980A impedance analysers (Wokingham, UK) over the frequency range 5 Hz to 10 MHz, with an *ac* measuring voltage of 0.1 V and over the temperature range –263 to 400 $^{o}$C; for subambient measurements, an Oxford Cryostat (Abingdon, UK) with Intelligent Temperature Controller (ITC 503S) was used. Impedance data were corrected for overall pellet geometry and for blank capacitance of the conductivity jig. Resistance values were obtained from intercepts on the real, Z' axis. Conductivity and capacitance data are reported in units of $Scm^{-1}$ and $Fcm^{-1}$, respectively, that refer to correction for only the overall sample geometry.

**Results and Discussion**

Results are presented for three sets of samples:

A) prepared by conventional reaction using a mortar and pestle to mix the powders and then fired at a final temperature of 850 °C for 2 hours;

B) prepared by mechanosynthesis and pellets sintered by heating to 850 °C at 10 °/min and then slow-cooled by switching off the furnace;

C) prepared by mechanosynthesis and pellets sintered by spark plasma sintering at 625 °C with or without a subsequent anneal at 600 °C in air for 2 hours.

Powder XRD data are shown for four typical samples in Fig. 1. The samples prepared by conventional solid state reaction (a) had $BiFeO_3$ as the major phase but with significant amounts of $Bi_2Fe_4O_9$ and $Bi_{25}FeO_{39}$ as secondary phases. It was found very difficult to eliminate these secondary phases either by repeated grinding and reheating or by pressing pellets and firing at different temperatures. By contrast, the samples prepared by mechanosynthesis (b, c, d) were essentially phase-pure and remained phase-pure in pellets sintered at 850 $^oC$ and also by SPS at 625 °C with or without a subsequent oxidative anneal at 600 °C. Before the mechanosynthesised samples were sintered, XRD lines were broadened due to small particle size and strain effects. Crystallite size calculated using the line profile analysis was ~16 nm. After sintering, XRD patterns of the mechanosynthesised samples were much improved without any secondary phases.

Lattice parameter data for the various samples are summarised in Table I together with typical literature values [26–28]. All samples were rhombohedral as expected. Rietveld refinement of sample (C) was carried out using powder XRD data and confirmed the correctness of the rhombohedrally-distorted perovskite structure of $BiFeO_3$; these results are summarised in Ref. 22.

DSC data are shown in Fig. 2 for samples prepared by (a) conventional reaction and (b) mechanosynthesis. Both show a weak transition at ~370 °C, which corresponds to the Néel temperature, $T_N$, for the phase transition from the antiferromagnetic low temperature polymorph to the paramagnetic high temperature polymorph. Both samples also show the ferroelectric to paraelectric transition at the Curie temperature, $T_C$, ~831 °C, with some hysteresis between heat and cool cycles, Table I.

Scanning electron micrographs are shown in Fig. 3 for mechanosynthesised powder, before (a) and after (b) conventional sintering and after SPS (c). The mechanosynthesised powder, (a), consisted of aggregates of fine particles. The particle sizes were typically 20 nm in size as confirmed by TEM

studies [22] (not shown) and are consistent also with the particle sizes obtained by line broadening of the XRD data, Fig. 1(b). The micrograph of the pellet sintered conventionally at 850 °C after mechanosynthesis, (b), shows a much larger grain size, typically 2.5–10 μm. This contrasts with the grain size of the pellet sintered by SPS, (c), which shows a more uniform texture with typical grain size 100 nm. An EDX spectrum of the SPS sample is shown in (d); analysis of the Bi:Fe atomic ratio gave a value of ~1 ; similar results were obtained by XRF [22] (not shown) for which the measured Bi:Fe atomic ratio was ~1.

Thermogravimetry measurements are shown in Fig. 4 for a pellet sintered conventionally and heated in vacuum at $5x10^{-5}$ mbars. The pellet shows a small decrease in mass over the temperature range ~75–325 $^{o}$C, no further mass change is observed until 650 $^{o}$C and on subsequent cooling. Moreover, thermogravimetric measurements in air did not show any mass loss in the same temperature range (figure not shown). XRD on a crunched pellet showed no evidence of secondary phases (not shown) and, therefore, the observed mass loss is likely to be associated with oxygen loss from the sample rather than sample decomposition during the TG experiment. Assuming that the air-processed sample is fully oxygenated, the oxygen loss in the formula $BiFeO_{3-\delta}$ is estimated as $\delta \approx 0.0326$; this value is somewhat higher than that reported previously by Li & MacManus-Driscoll [29] in which $BiFeO_{3-\delta}$ exhibits only a very narrow oxygen nonstoichiometry range, i.e. $\delta < 0.01$.

The conclusion from these various characterisation studies is that the samples produced by mechanosynthesis, and sintered either conventionally or by SPS, were well-crystallised, cation-stoichiometric $BiFeO_3$ but with a narrow oxygen nonstoichiometry range, without significant presence of impurity phases and exhibiting similar XRD and DSC data to those reported in the literature. This contrasts with the samples prepared by solid state reaction which contained small amounts of secondary phases, even after repeated heat treatments. All subsequent data reported here

used the pure-phase $BiFeO_3$ samples prepared by mechanosynthesis with either conventional or spark plasma sintering. All samples were electrically insulating at room temperature with $\sigma << 10^{-7}$ $Scm^{-1}$ but showed modest levels of semiconductivity at high temperatures.

Impedance data for $BiFeO_3$ sintered under various conditions are shown in Fig. 5 and 6. For mechanosynthesised samples sintered conventionally in air at 850 °C, Fig. 5, impedance complex plane plots (a) show a single, almost ideal, semicircular arc whose low frequency intercept give the total resistance of the sample. M″ and Z″ spectra (b) both show a single peak at almost coincident frequencies, which indicates the electrical homogeneity of the sample. Capacitance data (c) show a limiting high frequency plateau with an approximate value 10 $pFcm^{-1}$, corresponding to a permittivity of ~110 and which therefore represents the bulk response of the sample. At lower frequencies, an approximately linear, small increase in capacitance is observed, indicating a possible power law response. Conductivity, Y′, data (d) show a low frequency plateau that represent the sample bulk conductivity and a dispersion at higher frequencies indicating the onset of a possible power law response, i.e. Johnscher's "universal" power law; [30, 31] the origin of the power law has been attributed variously to atomic level interactions between ions or electrons within the material [31–35] and to the electrical response characteristics of two-phase, conductor–insulator, networks formed by the material's microstructure. [36–38] It is concluded that, to a first approximation, the electrical property data may be represented by the parallel R-C-CPE element shown in Fig. 5(a) inset, in which CPE is a Constant Phase Element responsible for the dispersion seen in both C′ data at low frequencies and Y′ data at high frequencies. Detailed analysis of the data and fitting to equivalent circuits has not been carried out.

For the mechanosynthesised sample sintered by SPS, an additional small low frequency arc is seen in the impedance complex plane plot, Fig. 6(a), which is not seen after the post-sinter oxidative anneal at 600 °C in air, Fig. 6(b). The data shown in Fig. 6(b,d) are similar to those seen in Fig. 5.

The additional arc seen at low frequencies in Fig. 6(a) appears in the C′ data (c) as a dispersion to a much higher capacitance value of ~5–10 nFcm$^{-1}$ at low frequencies and is attributed to grain boundaries in the ceramic, which are reduced to a different extent from the sample bulk. The effect of post-sinter anneal at 600 °C is to fully reoxidise both grain and grain boundary regions of the sample, as shown by impedance measurements carried out at a constant temperature after different time lapses, Fig. 7.

Fixed-frequency plots of relative permittivity ($\varepsilon'$) and tan δ against temperature are shown in Fig. 8 for $BiFeO_3$ prepared by mechanosynthesis and sintered by SPS at 625 ºC with a subsequent anneal in air at 600 °C. Relative $\varepsilon'$ data increase with temperature, as expected for a ferroelectric material on approaching $T_C$, and are frequency-dependent above ~200 $^{o}$C as a consequence of Johnscher's "universal" power law. Below ~175 ºC, $\varepsilon''$ and tan δ data are noisy since

$$\varepsilon'' = \left(Z'\omega\varepsilon_0\right)^{-1} \quad (1)$$

$$\tan\delta = \varepsilon''/\varepsilon' = \left(Z'\omega\varepsilon_0\varepsilon'\right)^{-1} \quad (2)$$

($\varepsilon_0$ = permittivity of free space, 8.854 $10^{-14}$ Fcm$^{-1}$ and ω = angular frequency, $2\pi f$) and the impedance of the sample was too large to be measured by the impedance analyser, i.e. $Z' >> 10^7$ Ωcm. Above ~175 ºC, the impedance of the sample was measurable and $\varepsilon''$ and tan δ data were frequency-dependent, as shown by equations (1) and (2).

Bulk conductivity data, $R^{-1}$, are shown in Arrhenius format in Fig. 9(a) for $BiFeO_3$ sintered conventionally: at 850 ºC in air followed by slow cooling; 800 $^{o}$C for 30 min in air followed by quenching; 350 $^{o}$C in vacuum at 5 $10^{-5}$ mbars followed by slow cooling; and 800 $^{o}$C for 1 h in high-pressure $O_2$ at ~125 bars (HOP) followed by slow cooling. The bulk resistivity at room temperature, extrapolated from the Arrhenius plots, is ~$10^{16}$ Ωcm with an activation energy for conduction of ~1.15–1.28 eV.

The difference in conductivity data between the four data sets is relatively small. The quenched and vacuum-annealed samples have lower conductivity than the slow-cooled sample which indicates that the charge carriers may be *p*-type electronic, i.e. holes ($h^{\bullet}$), since oxygen loss from the quenched or vacuum-annealed samples would lead to release of electrons:

$$2O_O^x \rightarrow O_2 + 2V_O^{\bullet\bullet} + 4e' \qquad (3)$$

and annihilation of hole charge carriers. An attempt to determine the principal conducting species by impedance measurements in different atmospheres at ~400 ºC shows a small increase in conductivity as the measuring atmosphere changes from nitrogen to air to oxygen, Fig. 10, which also suggests that the conduction mechanism may be slightly *p*-type, although the measured changes in conductivity are close to experimental error. This may be because conduction is nearly intrinsic but weakly dominated by holes. Possibly, thermopower measurements (not attempted) would be sufficiently sensitive to confirm the nature of the predominant charge carriers.

The SPS sample annealed at 600 °C had very similar conductivity to that of the conventionally sintered sample, Fig. 9(b). However, the SPS sample without the post-sinter anneal had higher conductivity and lower activation energy, i.e. 0.64(2) eV, indicating some reduction of the sample by the SPS process. Since the SPS sample is susceptible to reoxidation in air leading to a decrease in conductivity as a consequence of withdrawal of electrons from the sample [reverse of reaction (3)], the conduction mechanism in this sample is *n*-type electronic.

The bulk conductivity of $BiFeO_3$ sintered conventionally at 850 ºC in air followed by slow cooling and some reported *dc* [23, 39, 40] and bulk [41] conductivity data for BiFeO3 ceramics [23, 41] and a good-quality single crystal [39, 40] are compared in Fig. 9(c). The conductivity of the single crystal is ~2–3 orders of magnitude higher than that of the mechanosynthesised sample but the activation energy for conduction is comparable indicating a higher number of charge carries in the single crystal. By

contrast, reported data for ceramics [23, 41] exhibit high levels of electrical conductivity at room temperature, e.g. ~1x10$^{-5}$ Scm$^{-1}$, and low activation energy ~0.5 eV.

The origin of the semiconductivity in $BiFeO_3$ ceramics is commonly believed to be a consequence of oxygen loss during high temperature processing, with the resulting injection of electrons into the crystal lattice leading to *n*-type semiconductivity, equation (3). This presumably involves reduction of $Fe^{3+}$ to $Fe^{2+}$. However, our results show that, even in the highly reducing conditions during the SPS process, the oxygen loss from $BiFeO_3$ is small and ceramics are good insulators at room temperature.

A possible alternative source of semiconductivity could involve non-stoichiometry in $BiFeO_3$, i.e. $Bi_{1-x}FeO_{3-3/2}$ or $BiFe_{1-x}O_{3-3/2}$, as a consequence of Bi loss and/or a Bi or Fe deficiency, possibly arising from the decomposition of $BiFeO_3$ into e.g. $Bi_2Fe_4O_9$ and $Bi_{25}FeO_{39}$. Ionic mechanisms of charge compensation could involve creation of oxygen vacancies ($V_o^{\bullet\bullet}$) and either Bi vacancies ($Bi_{Bi}'''$) or Fe vacancies ($Fe_{Fe}'''$). Electronic charge compensation mechanisms could require hole creation to offset cation deficiency. Recently, it has been reported that the electrical properties of Ca-doped $BiFeO_3$ ceramics, i.e $Bi_{1-x}Ca_xFeO_{3-x/2+\delta}$, are controlled by the amount of oxygen ($\delta$) absorbed by the sample. [42] At room temperature, $Bi_{1-x}Ca_xFeO_{3-x/2+\delta}$ ceramics are good insulators if no absorption of oxygen occurs ($\delta \sim 0$) but show high levels of *p*-type semiconductivity on absorbing oxygen ($\delta >> 0$). In a similar way, the semiconductivity of $BiFeO_3$ ceramics may also be associated with non-stoichiometry followed by oxygen absorption leading to a hole conduction mechanism controlled by the schematic reaction:

$$2V_o^{\bullet\bullet} + O_2 \rightarrow 2O_O^x + 4h^{\bullet} \qquad (4)$$

or, alternatively,

$$2V_o^{\bullet\bullet} + O_2 + 4Fe_{Fe}^x \rightarrow 2O_O^x + 4Fe_{Fe}^{\bullet}, \qquad (5)$$

where holes may be associated with Fe, as $Fe^{4+}$ ions. At present, we cannot comment on the relative likelihood of these various possibilities.

In conclusion, we have shown here that high-quality $BiFeO_3$ ceramics, whose electrical properties are comparable to those of a good-quality $BiFeO_3$ single crystal, can be prepared by direct mechanochemical synthesis from pristine iron and bismuth oxides. The ceramics are highly insulating under all conditions, even those sintered by SPS at 650 $^oC$, and do not exhibit the high level of *n*-type semiconductivity frequently reported in the literature.

**Acknowledgments**

We thank Spanish Government (projects CTQ 2011-27626 and MAT 2008-06619), Junta de Andalucía (project TEP-03002), FEDER and EPSRC for financial support.

**References**

[1] C. Ederer and N. A. Spaldin, "Weak ferromagnetism and magnetoelectric coupling in bismuth ferrite", *Phys. Rev. B*, **71**[6] 060401(R) (2005).

[2] P. Fischer, M. Polomska, I. Sosnowska and M. Szymanski, "Temperature-dependence of the crystal and magnetic-structures of $BiFeO_3$", *J. Phys. C-Solid State Phy.*, **13**[10] 1931–1940 (1980).

[3] G. L. Yuan, S. W. Or, Y. P. Wang, Z. G. Liu and J. M. Liu, "Preparation and multi-properties of insulated single-phase $BiFeO_3$ ceramics", *Solid State Commun.*, **138**[2] 76–81 (2006).

[4] G. D. Achenbach, W. J. James, and R. Gerson, "Preparation of single-Phase polycrystalline $BiFeO_3$," *J. Am. Ceram. Soc.*, **50** [8] 437 (1967).

[5] S. Komarneni, V. C. Menon, Q. H. Li, R. Roy and F. Ainger, "Microwave-hydrothermal processing of $BiFeO_3$ and $CsAl_2PO_6$", *J. Am. Ceram. Soc.*, **79** [5] 1409–1412 (1996).

[6] S. Ghosh, S. Dasgupta, A. Sen and H. S. Maiti, "Low-temperature synthesis of nanosized bismuth ferrite by soft chemical route", *J. Am. Ceram. Soc.*, **88** [5] 1349–1352 (2005).

[7] C. Chen, J. Cheng, S. Yu, L. Che and Z. Meng, "Hydrothermal synthesis of perovskite bismuth ferrite crystallites", *J. Cryst. Growth*, **291**[1] 135–139 (2006).

[8] M. Valant, A. K. Axelsson and N. Alford, "Peculiarities of a solid-state synthesis of multiferroic polycrystalline $BiFeO_3$", *Chem. Mater.*, **19**[22] 5431–5436 (2007).

[9] V. Fruth, L. Mitoseriu, D. Berger, A. Ianculescu, C. Matei, S. Preda and M. Zaharescu, "Preparation and characterization of $BiFeO_3$ ceramic", *Prog. Solid State Ch.*, **35**[2–4] 193–202 (2007).

[10] M. Popa, D. Crespo, J. M. Calderon-Moreno, S. Preda and V. Fruth, "Synthesis and structural characterization of single-phase $BiFeO_3$ powders from a polymeric precursor", *J. Am. Ceram. Soc.*, **90** [9] 2723–2727 (2007).

[11] S. M. Selbach, M.-A. Einarsrud, T. Tybell and T. Grande, "Synthesis of $BiFeO_3$ by wet chemical methods", *J. Am. Ceram. Soc.*, **90** [11], 3430–3434 (2007).

[12] K. S. Nalwa, A. Garg and A. Upadhayaya, "Solid state synthesis and characterization of multiferroic $BiFeO_3$ ceramics", *Indian J. Eng. Mater. S.*, **15**[2] 91–94 (2008).

[13] A. Hardy, S. Gielis, H. Van den Rul, J. D'Haen, M. K.Van Bael and J. Mullens, "Effects of precursor chemistry and thermal treatment conditions on obtaining phase pure bismuth ferrite from aqueous gel precursors", *J. Eur. Ceram. Soc.*, **29**[14] 3007–3013 (2009).

[14] D. Maurya, H. Thota, K. S. Nalwa and A. Garg, "$BiFeO_3$ ceramics synthesized by mechanical activation assisted versus conventional solid-state-reaction process: A comparative study", *J. Alloy Compd.*, **477**[1-2) 780–784 (2009).

[15] J.-H. Xu, H. Ke, D.-C. Jia, W. Wang and Y. Zhou, "Low-temperature synthesis of $BiFeO_3$ nanopowders via a sol-gel method", *J. Alloy Compd.*, **472**[1–2] 473–477 (2009).

[16] X.B. He and L.A. Gao, "Synthesis of pure phase $BiFeO_3$ powders in molten alkali metal nitrates", *Ceram. Int.*, **35**[3] 975–978 (2009).

[17] T. Liu, Y. Xu and J. Zhao, "Low-temperature synthesis of $BiFeO_3$ via PVA sol–gel route", *J. Am. Ceram. Soc.*, **93**[11] 3637–3641 (2010).

[18] H. Zhang and K. Kajiyoshi, "Hydrothermal synthesis and size-dependent properties of multiferroic bismuth ferrite crystallites", *J. Am. Ceram. Soc.*, **93**[11] 3842–3849 (2010).

[19] T. Liu, Y. Xu, S. Feng and J. Zhao, "A facile route to the synthesis of $BiFeO_3$ at low temperature", *J. Am. Ceram. Soc.*, **94**[9] 3060–3063 (2011).

[20] K. L. Da Silva, D. Menzel, A. Feldhoff, C. Kübel, M. Bruns, A. Paesano, A. Düvel, M. Wilkening, M. Ghafari, H. Hahn, F. J. Litterst, P. Heitjans, K. D. Becker and V. Śepelák, "Mechanosynthesized $BiFeO_3$ nanoparticles with highly reactive surface and enhanced magnetization", *J. Phys. Chem. C*,. **115**[15] 7209–7217 (2011).

[21] I. Szafraniak, M. Połomska, B. Hilczer, A. Pietraszko, L. Kępińskic, "Characterization of $BiFeO_3$ nanopowder obtained by mechanochemical synthesis", *J. Eur. Ceram. Soc.*, **27**[13–15] 4399–4402 (2007).

[22] A. Perejón, N. Murafa, P.E. Sánchez Jiménez, J.M. Criado, J. Šubrt, M. J. Diánez, L. A. Pérez-Maqueda, "Direct mechanosynthesis of pure BiFeO3 perovskite nanoparticles with controlled microstructure: reaction mechanism", *J. Mater. Chem.*, submitted for publication.

[23] Y.-K. Jun, W.-T. Moon, C.-M. Chang, H.-S. Kim, H. S. Ryu, J. W. Kim, K. H. Kim, S.-H. Hong, "Effects of Nb-doping on electric and magnetic properties in multi-ferroic $BiFeO_3$ ceramics", *Solid State Commun.*, **135**[1–2] 133–137 (2005).

[24] K. Kalantari, I. Sterianou, S. Karimi, M. C. Ferrarelli, S. Miao, D. C. Sinclair and I. M. Reaney, "Ti-doping to reduce conductivity in $Bi_{0.85}Nd_{0.15}FeO_3$ Ceramics", *Adv. Funct. Mater.*, **21**[19] 3737–3743 (2011).

[25] P. E. Sánchez-Jiménez, A. Perejón, J. M. Criado, M. J. Diánez, L. A. Pérez-Maqueda, "Kinetic model for thermal dehydrochlorination of poly(vinyl chloride)", *Polymer*, **51**[17] 3998–4007 (2010).

[26] F. Kubel and H. Schmid, "Structure of a ferroelectric and ferroelastic monodomain crystal of the perovskite $BiFeO_3$", *Acta Cryst. B*, **46**[6] 698–702 (1990).

[27] C. Michel, J.-M. Moreau, G. D. Achenbach, R. Gerson and W. J. James, "The atomic structure of $BiFeO_3$", *Solid State Commun.*, **7**[9] 701–704 (1969).

[28] J. M. Moreau, C. Michel, R. Gerson and W.J. James, "Ferroelectric $BiFeO_3$ X-ray and neutron diffraction study", *J. Phys. Chem. Solids*, **32**[6] 1315–1320 (1971).

[29] M. Li and J. L. MacManus-Driscoll, "Phase stability, oxygen nonstoichiometry and magnetic properties of $BiFeO_3$", *Appl. Phys. Lett.* **87**[25] 252510 (2005).

[30] Jonscher A K in *Dielectric Relaxation in Solids*, Chelsea Dielectric Press, London, 1983.

[31] A. K. Jonscher in *Universal Relaxation Law*, Chelsea Dielectric Press, London, 1996.

[32] L A Dissado and R M Hill, "Anomalous low-frequency dispersion. Near direct current conductivity in disordered low-dimensional materials", *J. Chem. Soc., Faraday Trans. 2*, **80**[3] 291–319 (1984).

[33] J. C. Dyre "The random free-energy barrier model for AC conduction in disordered solids", *J. Appl. Phys.*, **64**[5] 2456–2468 (1988).

[34] J. C. Dyre and T. B. Schrøder, "Universality of AC conduction in disordered solids", *Rev. Mod. Phys.*, **72**[3] 873–892 (2000).

[35] K. Funke and R. D. Banhatti, "Ionic motion in materials with disordered structures", *Solid State Ionics*, **177**[19–25] 1551–1557 (2006).

[36] D. P. Almond and B. Vainas, "The dielectric properties of random R–C networks as an explanation of the 'universal' power law dielectric response of solids", *J. Phys.: Condens. Matter*, **11**[46] 9081–9093 (1999).

[37] D. P. Almond, C. R. Bowen and D. A. S. Rees, "Composite dielectrics and conductors: Simulation, characterization and design", *J. Phys. D Appl. Phys.*, **39**[7] 1295–1304 (2006).

[38] C. R. Bowen, D. P and Almond, "Modelling the 'universal' dielectric response in heterogeneous materials using microstructural electrical networks", *Mater. Sci. Tech.*, **22**[6], 719–724. (2006).

[39] R. Palai, R. S. Katiyar, H. Schmid, P. Tissot, S. J. Clark, J. Robertson, S. A. T. Redfern, G. Catalan, and J. F. Scott, "β phase and γ-β metal-insulator transition in multiferroic $BiFeO_3$", *Phys. Rev. B*, **77**[1] 014110 (2008).

[40] G. Catalan and J. F. Scott, "Physics and applications of Bismuth Ferrite", *Adv. Mater.*, **21**[24] 2463–2485 (2009).

[41] W.-T. Chen, A. J. Williams, L. Ortega-San-Martin, M. Li, D. C. Sinclair, W. Zhou and J. P. Attfield, "Robust antiferromagnetism and structural disorder in $Bi_xCa_{1-x}FeO_3$ perovskites", Chem. Mater., **21**[10] 2085–2093 (2009).

[42] N. Masó and A. R. West, "Electrical properties of Ca-doped $BiFeO_3$ ceramics: from *p*-type semiconduction to oxide-ion conduction", *Chem. Mater.*, **24**[11] 2127−2132 (2012).

**Table I.** Lattice parameters, cell volume (V), pellet density and $T_C$ for $BiFeO_3$.

| | Lattice parameters (Å) | | V (Å$^3$) | Pellet density (%) | $T_C$ ($^o$C) | |
|---|---|---|---|---|---|---|
| | *a* | *c* | | | heating | cooling |
| Conventionally prepared | 5.579(1) | 13.8694(16) | 373.89(12) | 85 | 834 | 818 |
| Direct mechanosynthesis | 5.58(2) | 13.83(5) | 372.9(3) | – | 830 | 810 |
| Mechanosynthesis and sintered at 850ºC | 5.5798(5) | 13.8724(1) | 374.05(7) | 92 | 831 | 813 |
| Mechanosynthesis and sintered by SPS at 625ºC | 5.579(2) | 13.869(4) | 373.8(2) | 97 | 831 | 816 |
| Ref 26. | 5.57874(16) | 13.8688(3) | 373.802(17) | | | |
| Ref 27. | 5.59 | 13.7 | 370.7 | | | |
| Ref 28. | 5.5876(3) | 13.867(1) | 374.93(5) | | | |

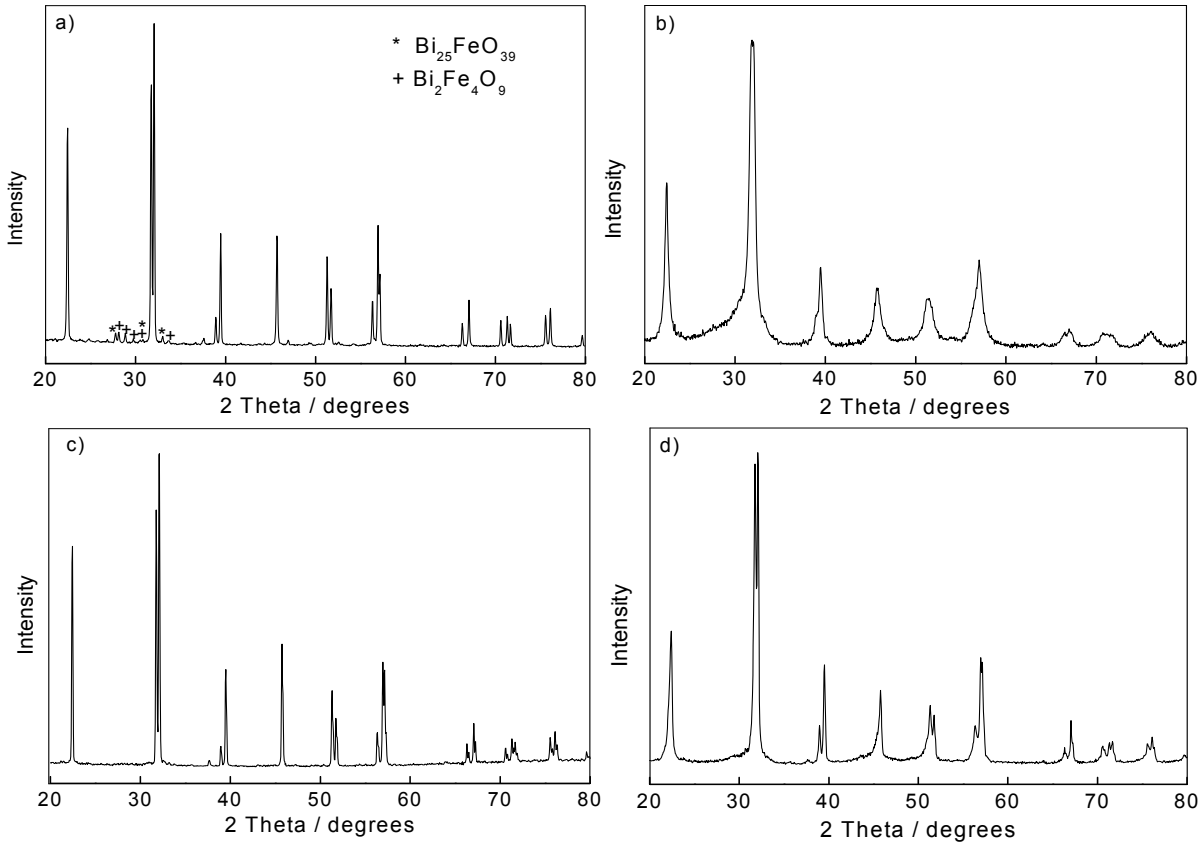


**Fig. 1.** XRD patterns for $BiFeO_3$ prepared by (a) conventional procedure (b) direct mechanosynthesis (c) mechanosynthesis and sintered at 850ºC and (c) mechanosynthesis and sintered by SPS. In (a), secondary phases are marked.

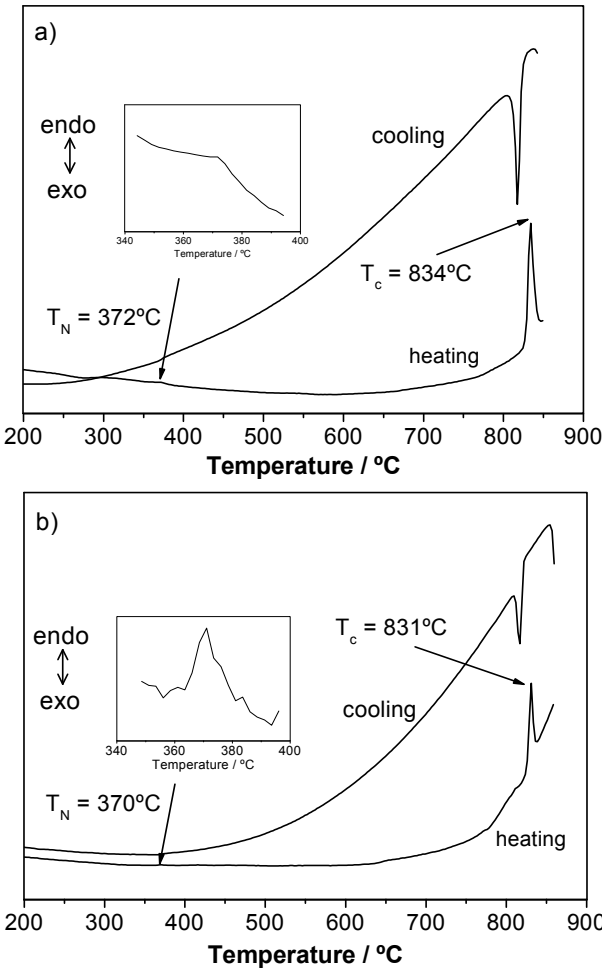


**Fig. 2.** DSC results for $BiFeO_3$ prepared by (a) conventional procedure (b) mechanosynthesis.

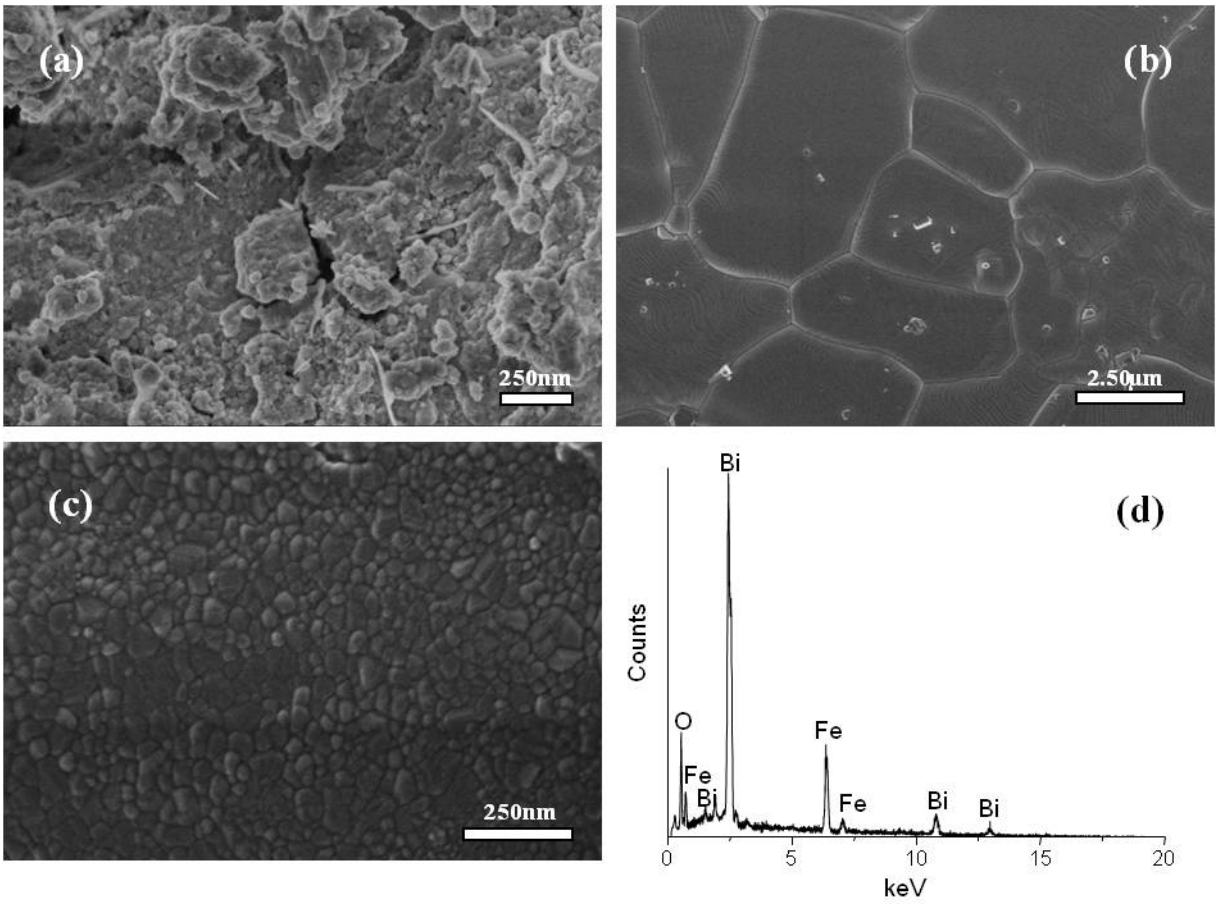


**Fig. 3.** SEM micrographs of (a) mechanosynthesized $BiFeO_3$ powder; (b) the pellet obtained after sintering at 850ºC; (c) the pellet obtained after sintering by SPS at 625ºC; (d) EDX analysis of the sample in (c).

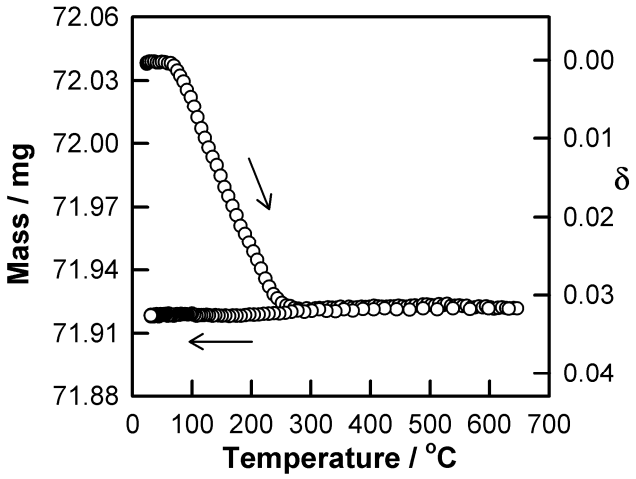


**Fig. 4.** Thermogravimetry measurements and oxygen loss (δ) in the formula $BiFeO_{3-\delta}$ for a pellet sintered conventionally and heated in vacuum at $5x10^{-5}$ mbars.

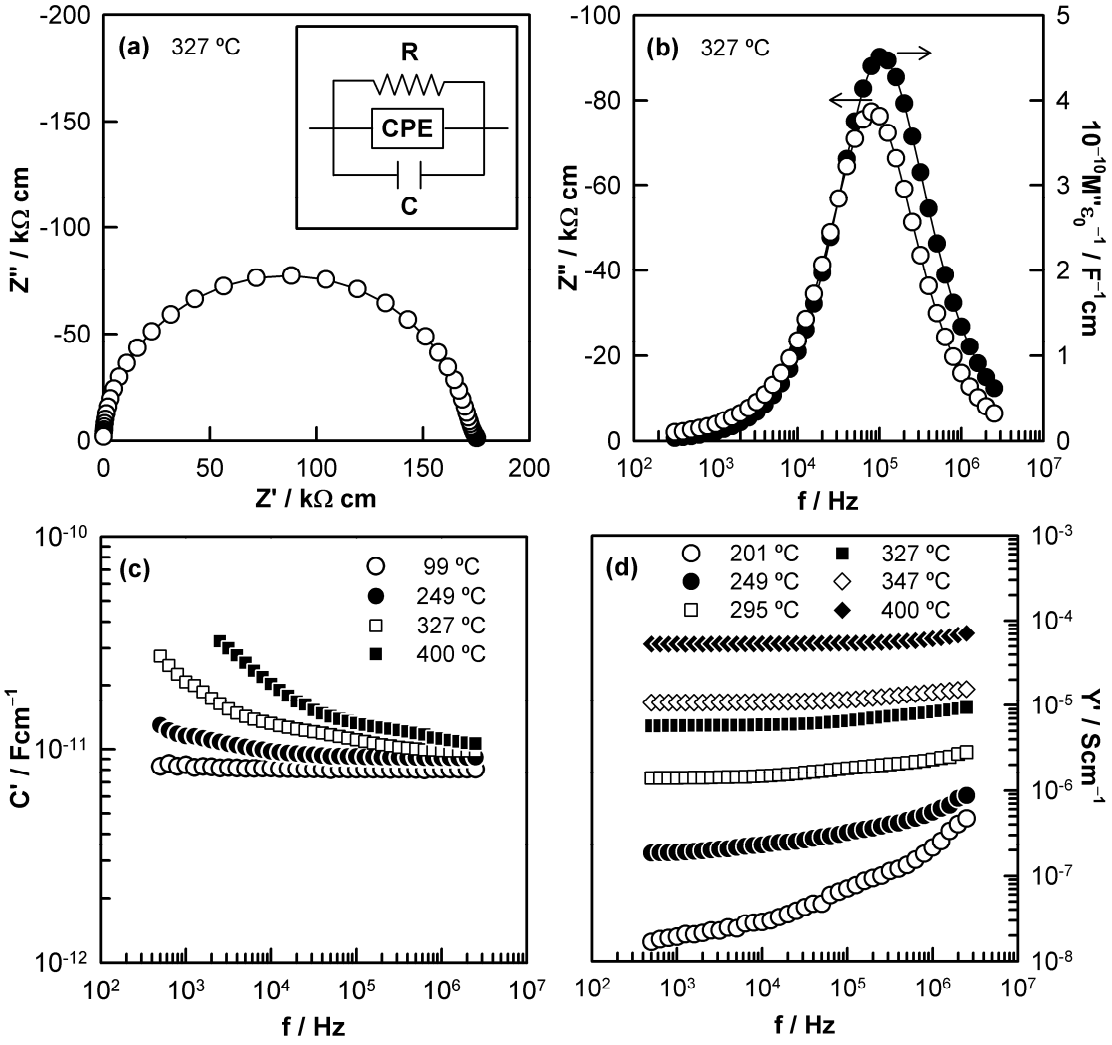


**Fig. 5.** (a) Impedance plots, (b) Z"/M" spectroscopic plots and (c) C' and (d) Y' *vs* frequency for $BiFeO_3$ obtained by mechanosynthesis and sintered at 850 ºC.

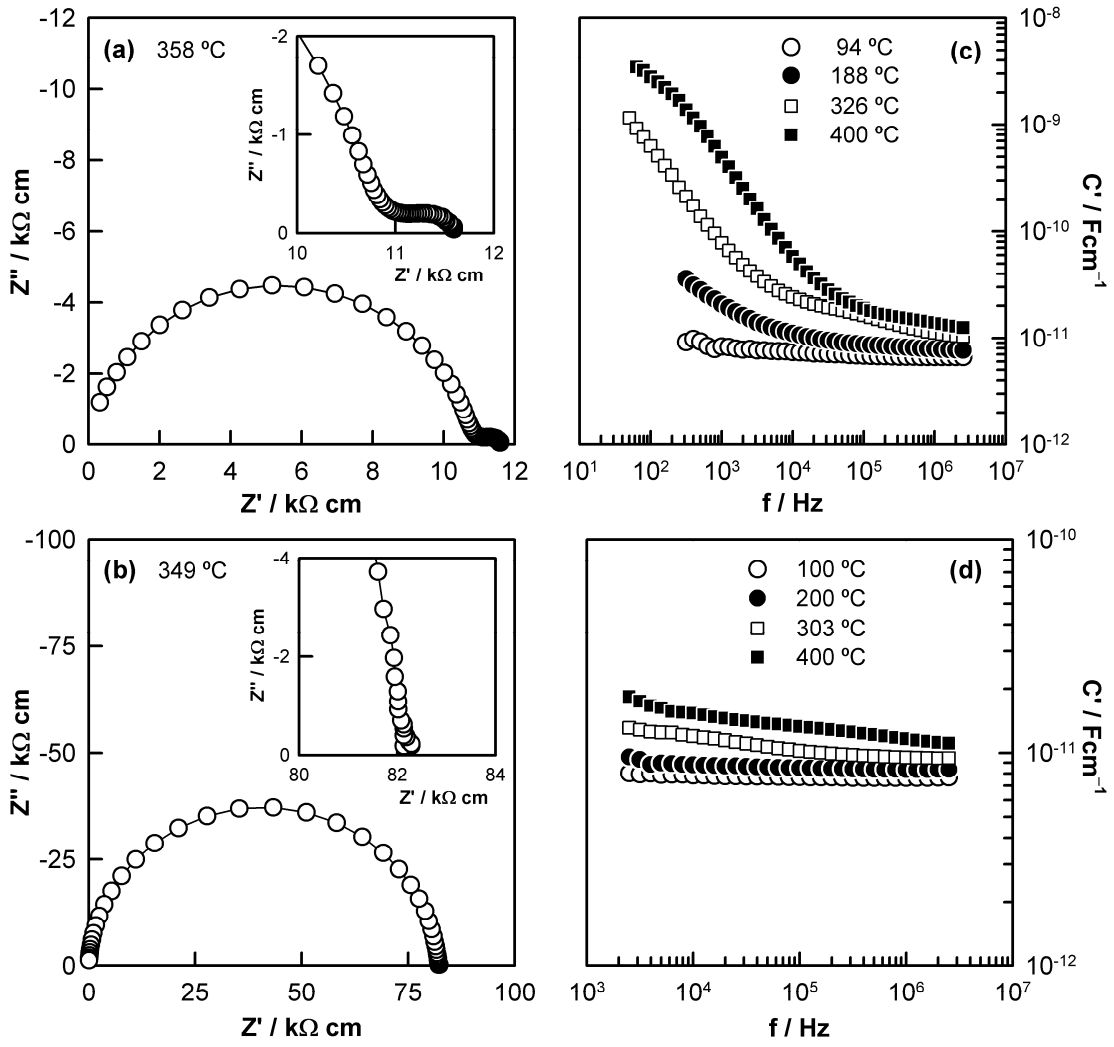


**Fig. 6.** (a, b) Impedance plots and (c, d) C' *vs* frequency for $BiFeO_3$ obtained by mechanosynthesis and sintered by SPS at 625ºC without (a, c) or with (b, d) a subsequent anneal at 600 °C in air for 2 hours. Data on the non-annealed sample were recorded in an atmosphere of $N_2$ to avoid sample oxidation during impedance measurements.

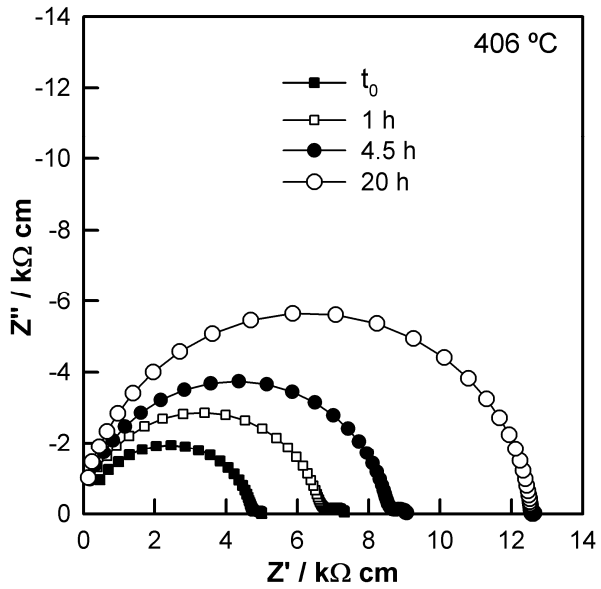


**Fig. 7.** Impedance complex plane plot for $BiFeO_3$, obtained by mechanosynthesis and sintered by SPS at 625 ºC, measured after different time lapses at 406 ºC.

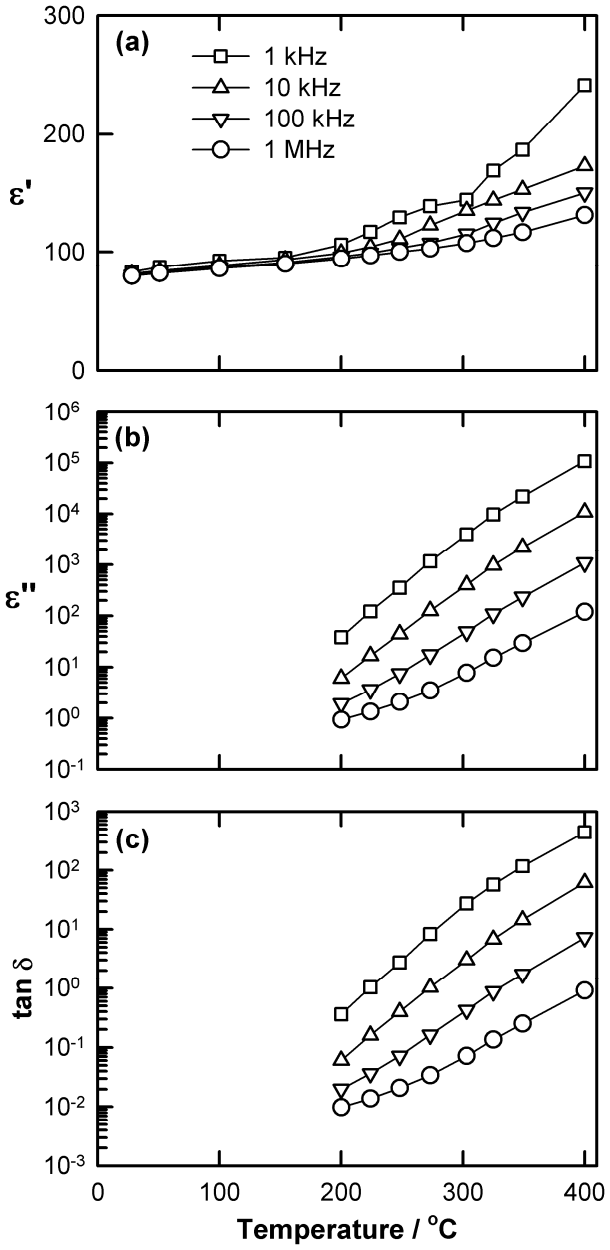


**Fig. 8.** Relative permittivity $(\varepsilon', \varepsilon'')$ and tan $\delta$ *vs* temperature of $BiFeO_3$ prepared by mechanosynthesis and sintered by SPS at 625 ºC with a subsequent anneal at 600 °C in air for 2 hours.

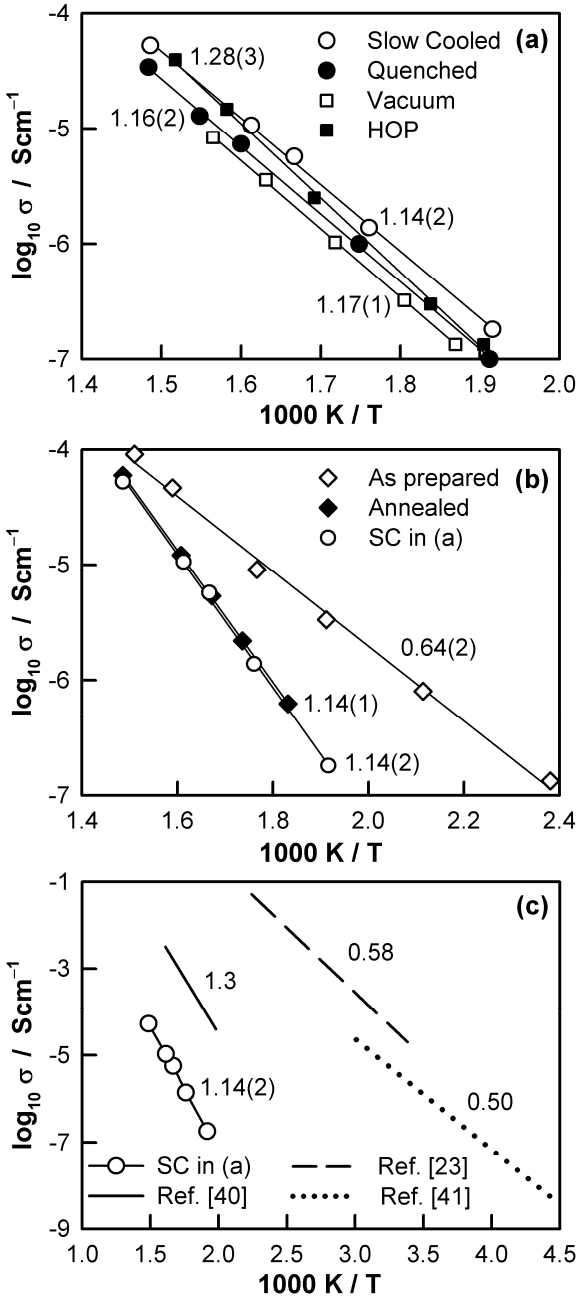


**Fig. 9.** Bulk Arrhenius plot for $BiFeO_3$ ceramics prepared by mechanosynthesis with conventional (a) and spark plasma (b) sintering with several processing conditions; and (c) comparison of reported conductivity data of $BiFeO_3$ ceramics [23, 41] and a single crystal. [40] Data for the slow cooled sample prepared by conventional sintering (SC) are shown for comparison in (b, c). Activation energies, in eV, are noted beside each data set.

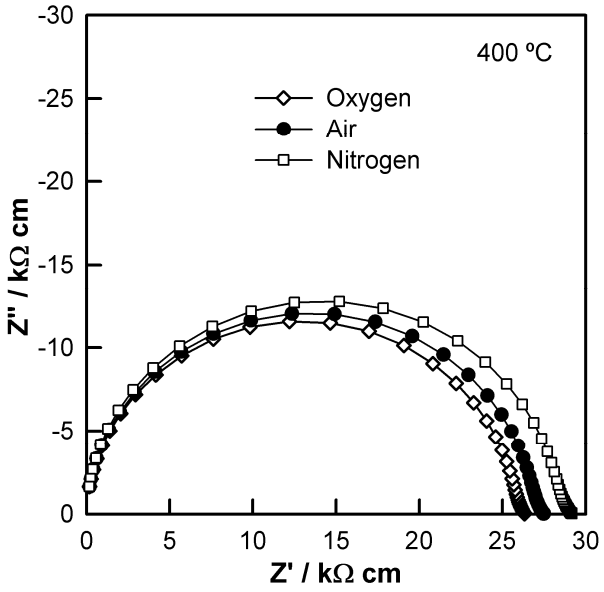


**Fig. 10.** Impedance complex plane plot for $BiFeO_3$, obtained by mechanosynthesis with conventional sintering at 850 ºC, measured in different atmospheres at 400 ºC.